

Kalman-Filter-Based Integer Ambiguity Resolution Strategy for Long-Baseline RTK with Ionosphere and Troposphere Estimation

Tomoji Takasu, Akio Yasuda
Tokyo University of Marine Science and Technology, Japan

revised 2010-10-03

BIOGRAPHY

Tomoji Takasu is a research fellow of Laboratory of Satellite Navigation at Tokyo University of Marine Science and Technology. He was working for developments of satellite systems at NEC Aerospace systems Ltd. from 1984 to 1997. He is currently involved in the research and development of precise positioning algorithms with GPS/GNSS, including PPP, RTK and INS/GPS integration.

Akio Yasuda graduated in 1966 from Dept. of Electrical Eng., Nagoya Institute of Technology, and obtained Dr. of Eng. degree from Nagoya University, and worked at Nagoya University and at Tokyo University of Mercantile Marine. Since 2004, he was Prof. at Tokyo University of Marine Science and Technology. He is currently conductor of Laboratory of Satellite Navigation. He was engaged in research on development of marine wave meter, BS and GMS reception onboard, regional positioning system with geostationary satellites. His concerning of GPS started in 1987. He is presently conducting the researches on multipath mitigation, analysis of ionospheric delay, improvement of RTK-GPS algorithm, and the other GPS related subjects. He is a member of IEICE (fellow), Japan Inst. Navigation, ION and IEEE.

ABSTRACT

The performance of RTK with long baseline over 100 km is much degraded compared to conventional short-range RTK. The authors have developed a new strategy for such long baseline RTK applicable to up to 1,000 km baselines. The strategy consists of an EKF-based parameter estimator without generating any linear combination of the measurements. The strategy also includes the integer ambiguity resolution in carrier-phase measurements with the partial fixing feature and tight constraints to once fixed integer ambiguities. To verify and demonstrate the proposed strategy, we conducted some online tests and

online real-time tests for the various baseline lengths in the range of from 29.9 km to 1,099.9 km. The results of these tests indicates that the proposed strategy works well up to 1,000 km baseline. The performance of such the long baseline RTK, however, is degraded especially in summer time. Further improvement is necessary to establish the strategy as a reliable and robust technique.

INTRODUCTION

RTK (real-time kinematic) is one of the most precise positioning technique with GNSS (global navigation satellite system). Users of RTK can easily obtain cm-level accuracy of user positions in real-time by using the measurements of GNSS signals received both at the user receiver and at the base station [1]. It is well known that the performance of RTK much depends upon baseline length defined as the distance between the user receiver and the base station. Table 1 shows the various lengths of baselines and RTK strategies applied to such baselines. In the case of RTK with a short baseline under 10 km, errors of satellite ephemerides, effects of ionosphere and troposphere are almost eliminated by forming DD (double-difference) measurement equations. With a medium length baseline under 100 km, in particular ionosphere effects are hard to be canceled by DD. In this case, dual-frequency measurements are often used to eliminate the ionosphere effects. With such a baseline range, it is also popular to cancel out the various error terms with corrections generated by interpolation of the residuals at multiple base stations around the user receiver. This network-RTK technique has been well verified and demonstrated by a lot of field experiments in previous researches [2]. At this moment, several commercial precise positioning services with GNSS based upon such the network-RTK systems have been already started and widely utilized by many users.

With a further longer baseline over 100 km, however, the RTK positioning still faces many difficulties compared to conventional ways mentioned above. The error terms in

Table 1: Baseline Lengths and RTK Strategies

Baseline Length		Error Elimination				RTK Strategy
		Ephemeris	Ionosphere	Troposphere	Other Errors	
Short	0 – 10 km	Broadcast	-	-	-	Conventional RTK
Medium	10 – 100 km	Broadcast	Dual-frequency	-	-	
			Interpolation		-	Network RTK
Long	100 – 1,000 km	Real-time precise (IGU)	Dual-frequency	Estimate ZTD+ mapping function	Earth tides	Long-baseline RTK
Very long	>1,000 km	Non-real-time precise (IGR, IGS)	Dual-frequency	Estimate ZTD+ mapping function	Earth tides, phase windup	Post-processing or PPP

the DD equation caused by broadcast ephemeris errors, troposphere delay and earth tides effects are not negligible for such a longer baseline. It is necessary to model the error terms carefully in measurement equation. Some of them are necessary to be estimated as additional unknown parameters. It is also hard to resolve integer ambiguities in the carrier-phase observables into proper values reliably and robustly due to these remaining errors. The longer initialization time is another issue especially to determine moving receiver's position in such long baseline RTK environment. A special integer ambiguity resolution strategy would be needed to reduce the initialization time under such condition.

Typical and promising applications of the long baseline RTK can be found on the sea. We usually can't find a fixed and stable base station for the short baseline RTK on vast ocean except nearby the coast. For example, the tsunami monitoring with GNSS has already been developed in Japan [3]. The system includes a GNSS-equipped buoy placed on open ocean. The buoy transmits GNSS observation data to a base station settled on the ground nearby the sea and the station computes precise buoy positions in real-time by using the RTK technique in order to detect coming tsunamis. The anchored point of such the buoy, however, is currently only under about 15 km apart from the coast. It is mainly because of the baseline length limitation of the conventional RTK technique. The limitation also forces need of a lot of GNSS buoys to cover all extended coast lines around the island. The shadowed area on the map in Figure 1 shows the coverage of the long baseline RTK near Japan, where we can find the nearest GNSS base station on the ground with 100–1,000 km baseline. As shown in the figure, if RTK provided sufficient and stable performance to measure precise variation of the buoys on the sea even with such long baseline, an very efficient tsunami warning system could be realized with minimum number of GNSS-buoys to mitigate tsunami disaster. The strong motivation of this research work is to develop

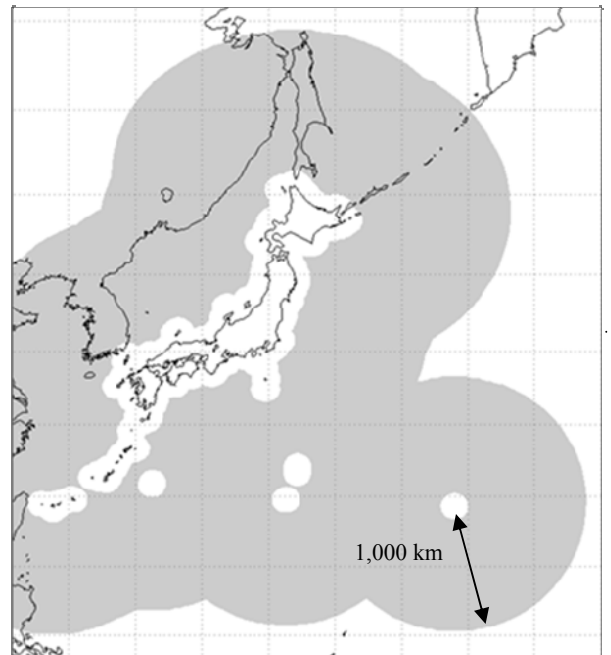


Figure 1. Area covered by long baseline RTK near Japan. The shadowed region indicates the area where we can find the nearest base station on the ground with 100–1,000 km baseline.

practical long baseline RTK technique for such promising applications.

INTEGER AMBIGUITY RESOLUTION FOR LONG BASELINE RTK

AR (ambiguity resolution) is a key technique to obtain rapid and precise solutions by RTK. In this section, firstly we briefly review the existing AR strategies for precise kinematic positioning with GNSS. Table 2 shows the various LCs (linear combinations) used for precise positioning with GNSS, where Φ_k and P_k show carrier-phase and pseudorange observables of L_k

frequency. For short baseline RTK, original observables L1, L2, P1 and P2 without LC are generally used to obtain the solutions. Recently many efficient and reliable algorithms have been developed as OTF (on the fly) AR technique for such the short baseline RTK. The most popular algorithm among them is well known as LAMBDA [4], which consists of the reduction step to shrink the search space of a integer vector by a linear transformation and the skillful tree search procedure of the integer vector under ILS (integer least square) condition. In the procedure, ionosphere effects in the measurement equations are assumed to be eliminated by double-differencing. It is hard to apply the strategy without any modification to long baseline RTK up to 1,000 km, where large ionosphere residuals remain.

On the other hand, for conventional medium or long baseline post-processing, so-called ionosphere-free LCs are often utilized. L3 shown in Table 2 indicates ionosphere-free LC of L1 and L2 carrier-phases, in which the ionosphere term is almost canceled. The ambiguity term, however, can't be separated into L1 and L2 terms. So it is impossible to resolve the carrier-phase ambiguity into an integer value without additional information. To resolve the ambiguity, another LC so-called MW (Melbourne-Wübbena) wide-line LC defined in Table 2 is often used. The LC cancels out not only the ionosphere term but also geometry and troposphere terms. So we can obtain an estimated integer wide-line ambiguity simply by averaging the LC and rounding the average to the nearest integer. Once the wide-lane ambiguity obtained, we can estimate the narrow-lane ambiguity as well as other unknown parameters with L3 LC measurement equations and the fixed wide-lane ambiguity. After that, the estimated narrow-lane ambiguity is also rounded to the nearest integer [5].

One of problems in applying such conventional

post-processing AR algorithm to the long baseline RTK is slow convergence time of the estimated ambiguity. Strictly speaking, the convergence time is a function of the reliability of the integer ambiguity resolved. To fasten the convergence time, the reliability decreases. To improve the reliability, the longer convergence time is needed. Assuming zero-mean Gaussian error distribution, theoretically, ILS condition assures the maximum probability to provide proper integer vector. The conventional sequential rounding scheme of wide-lane and narrow-lane ambiguities does not provide the optimum performance. To improve the conventional way, alternative ionosphere-free LCs as shown in Table 2 can be employed with the integer vector search under the ILS condition. However, the ionosphere-free LC also adds the measurement noise to the original measurement as shown in Table 2. It means that the error of the estimated user positions also increases especially in the kinematic mode. For the long baseline RTK, the strategy without LC is clearly better than that with LC.

Considering the problems of existing AR strategies as mentions above, we propose a new AR strategy for the long baseline RTK in this study. In this strategy, we form no linear combination and use only original observables of carrier-phases and pseudoranges in order to suppress the measurement noise. The ionosphere terms, which are not canceled by DD measurement equations in the case of the long baseline, are explicitly estimated as unknown parameters by EKF (extended Kalman filter) [6] as well as other unknowns. The estimated float ambiguities by EKF are resolved by existing efficient integer vector search strategy under ILS condition. For the integer vector search, we employs well known LAMBDA and its extension MLAMBDA [7] in this study.

Table 2. Various LCs (Linear Combinations) of GNSS Observables for Long Baseline Relative Positioning

Liner Combination	Coefficients of LC				Coefficients of Terms in DD Equation				Typical DD Noise σ (cm)	Notes
	Φ_1	Φ_2	P_1	P_2	$\rho + T$	I_1	N_1	N_2		
L1	λ_1				1	-1	λ_1		0.6	Original Observables
L2		λ_2			1	$-\gamma$		λ_2	0.6	
P1			1		1	1			60	
P2				1	1	γ			60	
L3	$C_1\lambda_1$	$C_2\lambda_2$			1	0	$C_1\lambda_1$	$C_2\lambda_2$	1.8	Ionosphere-Free LC
MW	λ_{WL}	$-\lambda_{WL}$	$-\lambda_{NL}/\lambda_1$	$-\lambda_{NL}/\lambda_2$	0	0	λ_{WL}	$-\lambda_{WL}$	42	
(L1+P1)/2	$\lambda_1/2$		1/2		1	0	$\lambda_1/2$		30	Alternative Ionosphere-Free LC
(L2+P2)/2		$\lambda_2/2$		1/2	1	0		$\lambda_2/2$	30	

$$\lambda_1 = 19.0 \text{ cm}, \lambda_2 = 24.4 \text{ cm}, \lambda_{WL} = 86.2 \text{ cm}, \lambda_{NL} = 10.7 \text{ cm}, \gamma = f_1^2 / f_2^2, C_1 = \gamma / (\gamma - 1), C_2 = -1 / (\gamma - 1)$$

EKF FORMULATION OF LONG BASELINE RTK

In this section, we introduce detailed formulations of EKF for the long baseline RTK with estimation of ionosphere and troposphere terms. By using EKF, a state vector \mathbf{x} and its variance-covariance matrix \mathbf{P} can be estimated with a measurement vector \mathbf{y}_k at an epoch t_k by:

$$\begin{aligned}\hat{\mathbf{x}}_k(+) &= \hat{\mathbf{x}}_k(-) + \mathbf{K}_k(\mathbf{y}_k - \mathbf{h}(\hat{\mathbf{x}}_k(-))) \\ \mathbf{P}_k(+) &= (\mathbf{I} - \mathbf{K}_k\mathbf{H}(\hat{\mathbf{x}}_k(-)))\mathbf{P}_k(-) \\ \mathbf{K}_k &= \mathbf{P}_k(-)\mathbf{H}(\hat{\mathbf{x}}_k(-))(\mathbf{H}(\hat{\mathbf{x}}_k(-))\mathbf{P}_k(-)\mathbf{H}(\hat{\mathbf{x}}_k(-))^T + \mathbf{R})^{-1}\end{aligned}\quad (1)$$

where $\mathbf{h}(\mathbf{x})$, $\mathbf{H}(\mathbf{x})$ and \mathbf{R} are the measurements model vector, the matrix of partial derivatives and the covariance matrix of measurement errors, respectively. Assuming the system-model linear, the time update of the state vector and its covariance by EKF is expressed as:

$$\hat{\mathbf{x}}_{k+1}(-) = \mathbf{F}_k^{k+1}\hat{\mathbf{x}}_k(+)$$

$$\mathbf{P}_{k+1}(-) = \mathbf{F}_k^{k+1}\mathbf{P}_k(+)\mathbf{F}_k^{k+1T} + \mathbf{Q}_k^{k+1}$$

where:

\mathbf{F}_k^{k+1} : state transition matrix from t_k to t_{k+1}

\mathbf{Q}_k^{k+1} : covariance matrix of system noise

For the long baseline RTK between the rover r and the base station b , the following measurement equations can be formed. In these equations, the satellite and receiver clock biases, satellite and receiver initial phases offsets in the carrier-phase observables are almost perfectly eliminated by double-differencing technique.

$$\Phi_{rb,k}^j \equiv \lambda_k \phi_{rb,k}^j = \rho_{rb}^j - I_{rb,k}^j + T_{rb}^j + \lambda_k (N_{rb,k}^i - N_{rb,k}^j) + \varepsilon_\phi$$

$$P_{rb,k}^j = \rho_{rb}^j + I_{rb,k}^j + T_{rb}^j + \varepsilon_p$$

where:

$()^j$: single-difference between satellite i and j

$()_{rb}$: single-difference between receiver r and b

$\phi_{r,k}^i$: L_k carrier-phase measurement (cycle)

$P_{r,k}^i$: L_k pseudorange measurement (m)

ρ_r^i : geometric range between satellite and receiver antenna phase center (m)

$I_{r,k}^i$: L_k ionosphere delay (m)

T_r^i : troposphere delay (m)

λ_k : L_k carrier wave length (m)

$N_{r,k}^i$: L_k carrier-phase ambiguity (cycle)

$\varepsilon_\phi, \varepsilon_p$: measurement errors of carrier-phase and pseudorange (m)

The unknown state vector \mathbf{x} for the long baseline RTK with dual-frequency GNSS observables is defined as:

$$\mathbf{x} = (\mathbf{r}_r^T, Z_{W,r}, G_{N,r}, G_{E,r}, Z_{W,b}, G_{N,b}, G_{E,b}, \mathbf{I}^T, N_1^T, N_2^T)^T \quad (4)$$

Note that single-difference is used instead of double-difference for carrier-phase ambiguities to avoid the hand-over problem of reference satellites. The measurement vector \mathbf{y} is also defined with double-differenced carrier-phase and pseudorange measurements as:

$$\mathbf{y} = (\Phi_1^T, \Phi_2^T, \mathbf{P}_1^T, \mathbf{P}_2^T)^T \quad (5)$$

$$\Phi_k = (\Phi_{rb,k}^{12}, \Phi_{rb,k}^{13}, \Phi_{rb,k}^{14}, \dots, \Phi_{rb,k}^{1m})^T$$

$$\mathbf{P}_k = (P_{rb,k}^{12}, P_{rb,k}^{13}, P_{rb,k}^{14}, \dots, P_{rb,k}^{1m})^T$$

By using equation (3), the measurement model vector $\mathbf{h}(\mathbf{x})$ and the matrix of partial derivatives $\mathbf{H}(\mathbf{x})$ can be written as:

$$\mathbf{h}(\hat{\mathbf{x}}) = (\mathbf{h}_{\phi,1}^T, \mathbf{h}_{\phi,2}^T, \mathbf{h}_{p,1}^T, \mathbf{h}_{p,2}^T)^T \quad (6)$$

$$\mathbf{h}_{\phi,k} = \begin{pmatrix} \rho_{rb}^{12} + T_{rb}^{12} - \gamma_k(m_1^1 I_{rb,1}^1 - m_1^2 I_{rb,1}^2) + \lambda_k(\hat{N}_{rb,k}^1 - \hat{N}_{rb,k}^2) \\ \rho_{rb}^{13} + T_{rb}^{13} - \gamma_k(m_1^1 I_{rb,1}^1 - m_1^3 I_{rb,1}^3) + \lambda_k(\hat{N}_{rb,k}^1 - \hat{N}_{rb,k}^3) \\ \vdots \\ \rho_{rb}^{1m} + T_{rb}^{1m} - \gamma_k(m_1^1 I_{rb,1}^1 - m_1^m I_{rb,1}^m) + \lambda_k(\hat{N}_{rb,k}^1 - \hat{N}_{rb,k}^m) \end{pmatrix}$$

$$\mathbf{h}_{p,k} = \begin{pmatrix} \rho_{rb}^{12} + T_{rb}^{12} + \gamma_k(m_1^1 I_{rb,1}^1 - m_1^2 I_{rb,1}^2) \\ \rho_{rb}^{13} + T_{rb}^{13} + \gamma_k(m_1^1 I_{rb,1}^1 - m_1^3 I_{rb,1}^3) \\ \vdots \\ \rho_{rb}^{1m} + T_{rb}^{1m} + \gamma_k(m_1^1 I_{rb,1}^1 - m_1^m I_{rb,1}^m) \end{pmatrix}$$

$$\rho_r^i = \|\mathbf{r}_r + \delta\mathbf{a}_r + \delta\mathbf{r}_{r,side} - \mathbf{r}^i - \delta\mathbf{a}^i\| + \delta p^i + \delta p_r$$

$$T_r^i = m_{H,r}^i Z_{H,r} + m_{WG,r}^i (Z_{T,r} - Z_{H,r})$$

$$m_{WG,r}^i = m_{W,r}^i \{1 + \cot El_r^i (G_{N,r} \cos Az_r^i + G_{E,r} \sin Az_r^i)\}$$

$$\gamma_k = \lambda_k^2 / \lambda_1^2$$

$$\mathbf{H}(\hat{\mathbf{x}}) = \left. \frac{\partial \mathbf{h}(\mathbf{x})}{\partial \mathbf{x}} \right|_{\mathbf{x}=\hat{\mathbf{x}}} = \begin{pmatrix} -DE & \mathbf{DM}_{T,r} & \mathbf{DM}_{T,b} & -\gamma_1 \mathbf{DM}_I & \lambda_1 \mathbf{D} \\ -DE & \mathbf{DM}_{T,r} & \mathbf{DM}_{T,b} & -\gamma_2 \mathbf{DM}_I & \lambda_2 \mathbf{D} \\ -DE & \mathbf{DM}_{T,r} & \mathbf{DM}_{T,b} & \gamma_1 \mathbf{DM}_I & \\ -DE & \mathbf{DM}_{T,r} & \mathbf{DM}_{T,b} & \gamma_2 \mathbf{DM}_I & \end{pmatrix} \quad (7)$$

$$\mathbf{E} = (\mathbf{e}_r^1, \mathbf{e}_r^2, \dots, \mathbf{e}_r^m)^T$$

$$\mathbf{M}_{T,r} = \begin{pmatrix} m_{WG,r}^1 & m_{W,r}^1 \cot El_r^1 \cos Az_r^1 & m_{W,r}^1 \cot El_r^1 \sin Az_r^1 \\ m_{WG,r}^2 & m_{W,r}^2 \cot El_r^2 \cos Az_r^2 & m_{W,r}^2 \cot El_r^2 \sin Az_r^2 \\ \vdots & \vdots & \vdots \\ m_{WG,r}^m & m_{W,r}^m \cot El_r^m \cos Az_r^m & m_{W,r}^m \cot El_r^m \sin Az_r^m \end{pmatrix}$$

$$\mathbf{M}_I = (m_1^1, m_1^2, \dots, m_1^m)^T$$

where:

\mathbf{r}^i : satellite i center of mass position (m)

$\delta\mathbf{a}^i$: satellite i antenna phase center offset (m)

δp^i : satellite i antenna phase variation (m)

\mathbf{r}_r : receiver r antenna position (m)

δa_r : receiver r antenna phase center offset (m)
 $\delta r_{r,tide}$: receiver r displacement by earth tides (m)
 δp_r : receiver r antenna phase center variation (m)
 e_r^i : unit LOS (line-of-sight) vector from receiver r to satellite i
 Az_r^i, El_r^i : azimuth and elevation of satellite i from receiver r (rad)
 $Z_{T,r}$: tropospheric zenith total delay (m)
 $Z_{H,r}$: tropospheric zenith hydrostatic delay (m)
 $G_{E,r}$: east component of tropospheric gradient
 $G_{N,r}$: north component of tropospheric gradient
 $m_{H,r}^i, m_{W,r}^i$: mapping function for hydrostatic and wet tropospheric delay
 m_i^i : mapping function for ionospheric delay
 $I = (I_{rb,1}^1, I_{rb,1}^2, \dots, I_{rb,1}^m)^T$: single-differences of L_1 vertical ionospheric delay (m)
 $N_{L_j} = (N_{rb,L_j}^1, N_{rb,L_j}^2, \dots, N_{rb,L_j}^m)^T$: single-differences of L_j carrier-phase ambiguities (cycle)

$$D = \begin{pmatrix} 1 & -1 & 0 & \dots & 0 \\ 1 & 0 & -1 & \dots & 0 \\ \vdots & \vdots & \vdots & \ddots & \vdots \\ 1 & 0 & 0 & \dots & -1 \end{pmatrix} : \text{single-differencing matrix}$$

The covariance matrix of the double-differenced measurement errors is also expressed as:

$$R = \begin{pmatrix} DR_{\phi,1}D^T & & & \\ & DR_{\phi,2}D^T & & \\ & & DR_{p,1}D^T & \\ & & & DR_{p,2}D^T \end{pmatrix} \quad (8)$$

$$R_{\phi,k} = \text{diag}(2\sigma_{\phi,k}^1{}^2, 2\sigma_{\phi,k}^2{}^2, \dots, 2\sigma_{\phi,k}^m{}^2)$$

$$R_{p,k} = \text{diag}(2\sigma_{p,k}^1{}^2, 2\sigma_{p,k}^2{}^2, \dots, 2\sigma_{p,k}^m{}^2)$$

where:

$\sigma_{\phi,k}^i, \sigma_{p,k}^i$: standard deviation of L_k carrier-phase and pseudorange measurement error (m)

The time update of EKF is expressed by equation (2) with:

$$F = I, Q = \begin{pmatrix} \infty_{3 \times 3} & & & \\ & Q_r & & \\ & & Q_i & \\ & & & 0_{32 \times 32} \end{pmatrix} \quad (9)$$

where:

$\tau_r = t_{k+1} - t_k$: receiver sampling interval (s)
 $\sigma_{ve}, \sigma_{vn}, \sigma_{vu}$: standard deviations of east, north and up component of the rover velocity system noise (m/ \sqrt{s})
 Q_i, Q_r : covariance of process noise for ionosphere and

troposphere terms

By solving the EKF formula (1), (2) with the RTK-GPS equation (4)-(9), the estimated rover antenna position, velocity and float carrier-phase ambiguities can be obtained.

In the strategy, the estimated states by EKF include the rover receiver ECEF position, single-differenced slant ionospheric delay for each satellites, tropospheric ZWD (zenith wet delay) and gradient parameters at the rover and base-station sites and float ambiguities for dual-frequency carrier-phases. It intends to utilize real-time precise satellite orbit provided IGS to suppress the ephemeris errors. It also uses single-layer MF (mapping function) for ionosphere and popular NMF for troposphere. The temporal variations of the ionosphere and troposphere terms are simply modeled as random-walk.

After obtaining the float estimated states by EKF, we transform the single-differenced ambiguities to double-differenced form as:

$$\hat{x}'_k = G \hat{x}_k(+) = (R^T, \hat{N}^T)^T$$

$$P'_k = GP_k(+)G^T = \begin{pmatrix} Q_R & Q_{NR} \\ Q_{RN} & Q_N \end{pmatrix} \quad (10)$$

$$G = \begin{pmatrix} I & \\ & D \\ & & D \end{pmatrix}$$

In this forms, the best integer vector \tilde{N} for the double-differenced carrier-phase ambiguities is searched to satisfy the condition of ILS (integer least square) problem as:

$$\tilde{N} = \underset{N \in Z}{\text{argmin}} ((N - \hat{N})^T Q_N^{-1} (N - \hat{N})) \quad (11)$$

To solve the problem, a well-known efficient strategy LAMBDA and its extension MLAMBDA are employed in this study. After the validation by the simple ratio-test, the fixed solution of the real parameter vector R including the rover position are obtained by solving the following equation.

$$\tilde{R} = \hat{R} - Q_{RN} Q_N^{-1} (\hat{N} - \tilde{N}) \quad (12)$$

IMPROVMENT OF FIXING RATIO

According to the details described in previous section, we implemented the long baseline RTK strategy and made

some tests with real measurement data. With simple implementation, however, we did not obtain adequate performance for both initialization time and fixing ratio. Figure 1 shows an example of the result with 300 km baseline by simple implementation of the strategy. The upper plots indicate E/N/U components of the solutions errors. The green dots show the fixed solutions after the validation by the ratio-test with the critical value of 3. The E/N/U standard deviations of the solutions are 2.2 cm, 2.3 cm and 3.2 cm respectively. The fixing ratio is only 46.4 %.

Such low fixing ratio seems mainly due to the satellites which are newly rising from the horizon. The carrier-phase ambiguities for such satellites usually need longer convergence time after they firstly become visible especially in longer baseline environment. The un-converged ambiguities often disturb the other ambiguity fixing by search type AR strategy under ILS condition, which assumes all of ambiguities are resolved together at the same time. If some estimated float ambiguities have large residuals, the validation process rejects the fixed solution because of biased. Not all the ambiguities, however, must be fixed in the same time. It is just a trade-off problem between the accuracy of the solutions and the fixing ratio.

To improve the situation, "partial fixing" strategy is introduced in this study. It means that only the some partial portion of all ambiguities are resolved into integer values. Other ambiguities except for the fixed are still pending as float values. Some criteria to decide whether a ambiguity should be fixed or float can be considered. The criteria include the variance of estimated ambiguity, duration of continuous valid data and so on. After some experimental evaluations for the issue, we decided to

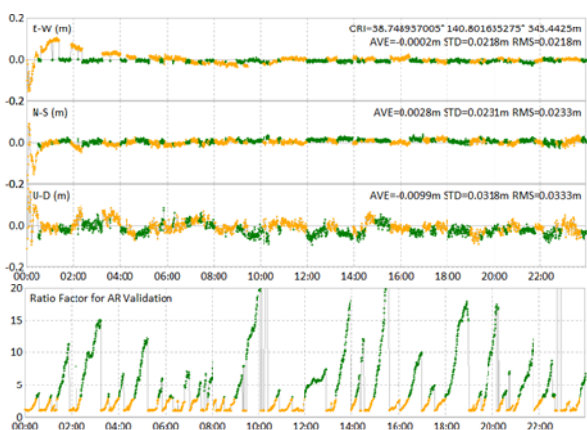


Figure 1. E/N/U errors (upper) and ratio factor of ratio-test (lower) with 300 km baseline by simple implementation of proposed long baseline RTK strategy

employ a very simple criterion involving the satellite elevation angle. If a satellite is under a threshold of the elevation, the ambiguities of the satellite are not fixed. Only the ambiguities of satellites over the threshold are resolved to integer. In this scheme, we can separate the ill-conditioned ambiguities and hold them as float values. The partial fixing improves availability of (partially-) fixed solutions in exchange for a little degradation of the accuracy of the solutions.

Another improvement is "fix and hold" mode for integer ambiguity resolution. That means tight constraint to fixed ambiguities. At first, estimated float ambiguities are resolved by the usual way but once the integer solutions are verified by the validation process, the tight constraint to the integer solutions is introduced into the next update of the filter. An fixed ambiguity is held to an integer value until a cycle-slip occurs or the filter diverged with large residuals. We call this behavior "fix and hold" mode. We expected these features much improve the initialization time and the fixing ratio for long-baseline RTK.

Figure 2 shows the results by the improved long baseline RTK strategy including "partial fixing" and "fix and hold mode". The E/N/U standard deviation of the solution are 1.1 cm, 1.9 cm and 3.5 cm respectively. The fixing ratio is much improved to 99.3 %. The figure clearly shows the proposed strategies are effective to enhance the initialization performance and fixing probability.

IMPLEMENTATION OF LONG BASELINE RTK

According to the strategy described in previous sections, we implemented the algorithm of the long baseline RTK. We already have RTKLIB, which is an open source

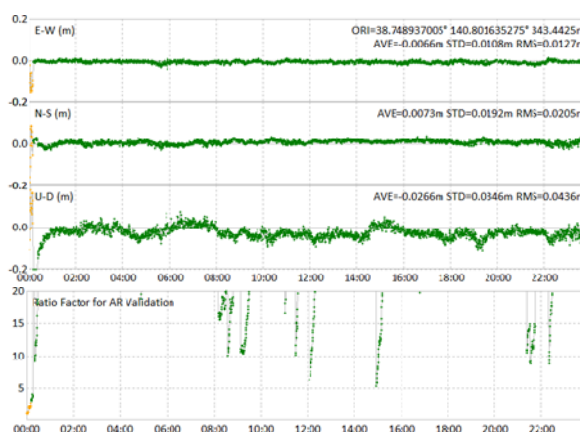


Figure 2. E/N/U errors (upper) and ratio factor of ratio-test (lower) with 300 km baseline by improved long baseline RTK strategy with "partial fixing" and "fix and hold mode". The threshold of the elevation to fix ambiguities is set to 25°.

program package for RTK developed by the authors [8]. RTKLIB already supports various standard messages defined by RTCM v.2 [9] or RTCM v.3 [10], and proprietary message formats supported by some GNSS receivers. The raw observation data streams of the rover and the base station can be input from remote sites via Internet by using standard TCP/IP or NTRIP [11] for the RTK positioning in real-time.

We also implemented some features in RTKLIB to support the long baseline RTK in addition to the RTK strategy itself mentioned above. The features include the handling of IGS [12] real-time precise orbit (IGS ultra-rapid ephemeris) and the automatic download of the SP3-c files of the precise ephemeris from the IGS data server. For the test and the evaluation, we also implemented the long baseline RTK strategy in post-processing mode as well as in real-time mode. We can input observation data and navigation data of the rover and the base station as standard RINEX [13] files and obtain the post-processing solutions as same as in real-time. The latest version of RTKLIB used for the evaluation was 2.4.1b. The stable version of RTKLIB supporting such long baseline RTK strategy will be released still as an open source program package by the end of 2010 at the web site for RTKLIB [14].

OFFLINE TEST OF LONG BASELINE RTK

To verify and evaluate the performance of the proposed long baseline RTK strategy, we conducted some experiments. At first, we made the offline test by using the post-processing mode with various lengths of baselines up to 1,100 km. We gathered RINEX observation data of GEONET, which is the Japanese dense CORS (continuous operating reference stations) network containing over 1,200 GNSS tracking stations distributed all over Japan [15]. Among all of the GEONET stations, we selected 2110 Tsukuba1 for the base station located around the center of Japanese island. We also selected 477 GEONET stations for the rover and formed 477 baselines between the rovers and the base station. The baseline lengths were distributed from 29.9 km to 1,099.9 km. Figure 2 shows the locations of such GEONET stations and the baselines for the offline test.

For the offline test, we used RTKLIB AP (application program) RTKPOST. RTKPOST supports various positioning mode including the carrier-phase based relative kinematic positioning as same as the algorithm for the long baseline RTK described above. We input RINEX observation data and navigation data received at the selected GEONET stations to RTKPOST. Concerning the satellite ephemeris, we downloaded the IGS (IGS

ultra-rapid) precise ephemeris and extracted only the predicted part from the SP3 file. The detailed option settings for RTKPOST are summarized in Table 3. To investigate the seasonal variation of the RTK performance, we used two data sets for the offline test.

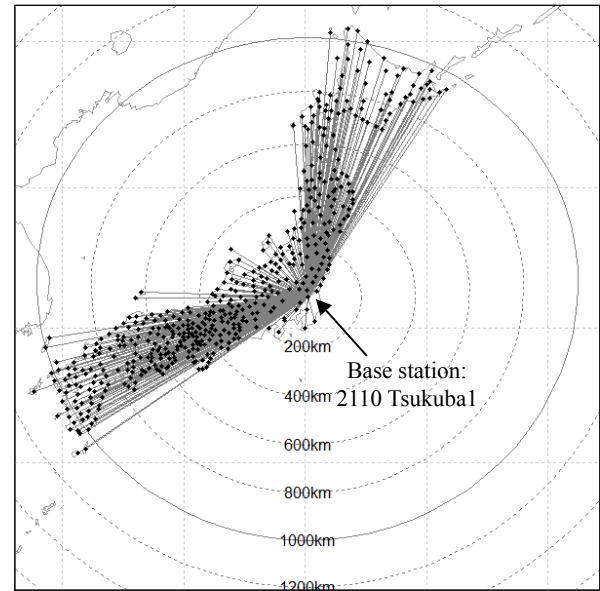


Figure 3. Baselines for offline test of long-baseline RTK Circles show the distances from the base-station 2110 Tsukuba 1

Table 3. Option settings of RTPOST for the offline test to evaluate proposed long baseline RTK strategy

Option	Setting
Positioning Mode	Kinematic
Frequencies	L1+L2
Receiver Dynamics	OFF
Earth Tides Correction	ON
Elevation Mask	7°
Ionosphere Correction	Estimate STEC
Troposphere Correction	Estimate ZTD + Gradient
Satellite Ephemeris	Precise
Ambiguity Validation Threshold	3.0
Min Elevation to Fix Ambiguity.	25°
Min Elevation to Hold Ambiguity	35°
Code/Carrier-Phase Error Ratio	100
Carrier Phase Error	$0.003 + 0.003 / \sin E_l$ m
Process Noise of Vertical Iono. Delay	10^{-3} m / sqrt(s)
Process Noise of ZTD	10^{-4} m / sqrt(s)
Satellite Antenna Model	IGS05.ATX
Receiver Antenna Model	IGS05.ATX

One was a week data on January 1-7, 2009 for the test in winter. Another was the same duration data set on July 1-7, 2009 for summer. The sampling interval of the

measurements for the both data sets was 30 s. Note that 2009 was the a silent year in terms of solar activity. The ionospheric condition might be fine compared to the averaged year. The performance of the long baseline RTK would be much degraded with ionosphere disturbance induced by higher solar activity.

Figure 4 shows an example of the test result as the errors of position solutions with a 471.2 km baseline. The east,

north and up standard deviation were 0.7 cm, 0.9 cm and 2.3 cm for the January data set, and 1.1 cm, 1.3 cm and 3.8 cm for the July data set, respectively. The fixing ratio were also 99.8 % and 99.0%, respectively. Figure 5 shows all of the offline test results of the winter case as the plot of standard deviations and fixing ratios corresponding to the baseline lengths. Figure 6 also shows the results of summer case. Table 4 summarize the offline test results as the averaged fixing ratio and standard deviation of 477

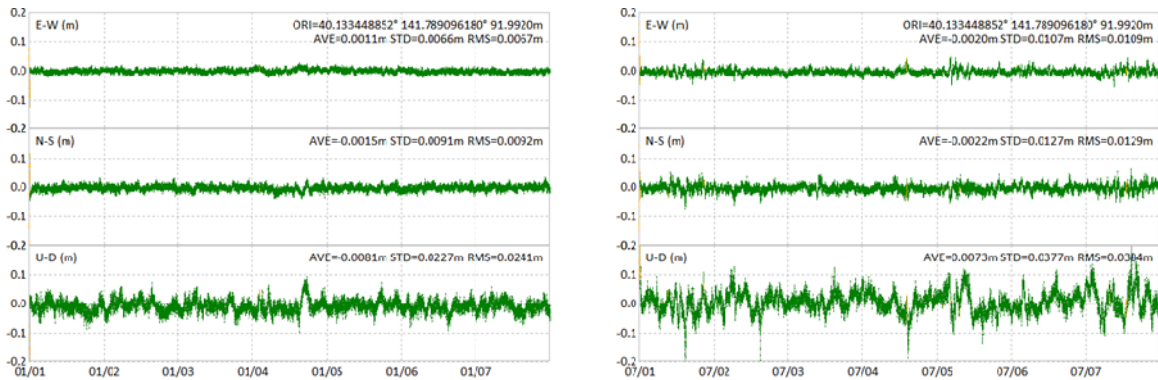


Figure 4. E/N/U errors of the offline test results for long baseline RTK strategy with 471.2 km baseline (left: January 1-7, 2009, right: June 1-7, 2009),

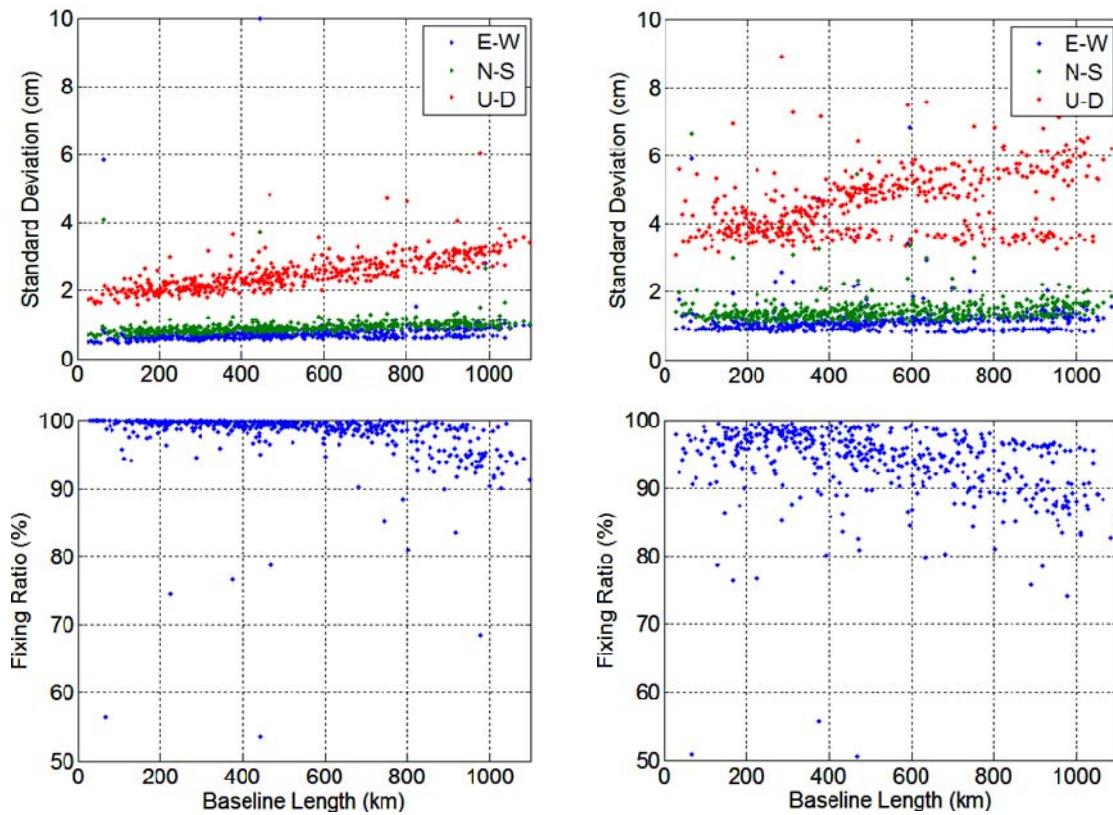


Figure 5. Standard deviation (upper) and fixing ratio (lower) of the offline test results for the long-baseline RTK strategy corresponding to their baseline lengths (left: January 1-7, 2009, right: June 1-7, 2009)

baselines.

As shown in the table, the proposed strategy for long baseline RTK seems to work well even over 1,000 km baseline. However the RTK performance both of the standard deviation and fixing ratio clearly degraded in summer season compared to in winter especially with longer baselines over 500 km. The maximum water vapor content in atmosphere increases due to higher temperature in summer. The larger variation of such water vapor content might cause the large errors in tropospheric corrections and degrade the long baseline RTK performance. More strict and fine modeling of troposphere is necessary to improve the performance for summer season.

Table 4. Summary of results of the offline test of the long-baseline RTK

Data Set	Average of Fixing Ratio	Average of Standard Deviation		
		E-W	N-S	U-D
January 1-7, 2009	97.8%	0.7 cm	0.9 cm	2.6 cm
July 1-7, 2009	93.4%	1.4 cm	1.6 cm	5.2 cm

REAL-TIME TEST OF LONG BASELINE RTK

To evaluate and demonstrate the proposed strategy for the long baseline RTK in real-time environment, we also conducted the real-time test. Figure 6 shows the configuration of the real-time test. For the test, NovAtel dual-frequency GNSS antenna and receiver were used as the rover receiver. IGS MIZU and SUWN real-time stations were used for the base stations. Figure 7 shows the locations of the rover receiver and the base stations. The baseline lengths were 435.7 km and 1,024.8 km for

the base station MIZU and SUWN, respectively. The real-time AP RTKNAVI in RTKLIB ver. 2.4.1b was installed in a PC and used as the real-time RTK client software the test. RTKNAVI connected by NTRIP ver. 1.0 protocol to BKG NTRIP broadcaster provided by IGS to receive the real-time streams of 1Hz base station data in RTCM ver. 3.1 type 1004 messages. RTKNAVI also automatically download the newest IGS ultra-rapid (IGU) precise ephemeris (IGU) from NASA GSFC CDDIS server every 6 hours. The real-time test was conducted for 72 hours from 12:00 GPST on September 17, 2010 to 12:00 GPST on September 20, 2010.

Figure 8 shows the real-time test results as the E/N/U error plot of solutions for both of 435.7 km and 1024.8 km baseline cases. The E/N/U standard deviations were 3.0 cm, 2.7 cm and 7.4 cm for the 435.7 km baseline and 3.3 cm, 2.9 cm and 7.9 cm for the 1024.8 km baseline. The fixing ratio are 93.5 % and 56.9 %, respectively.

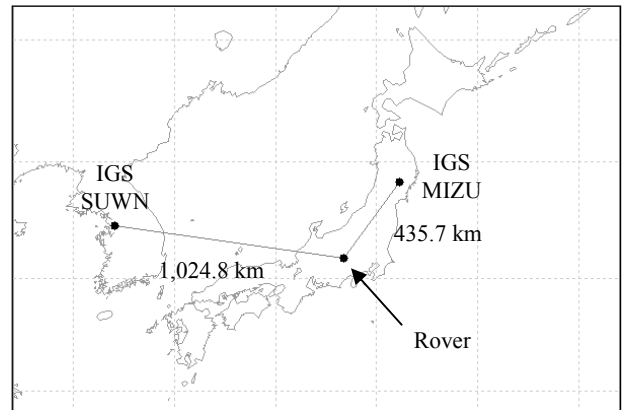


Figure 7. Locations of the rover and the base stations for the real-time test for the long baseline RTK strategy.

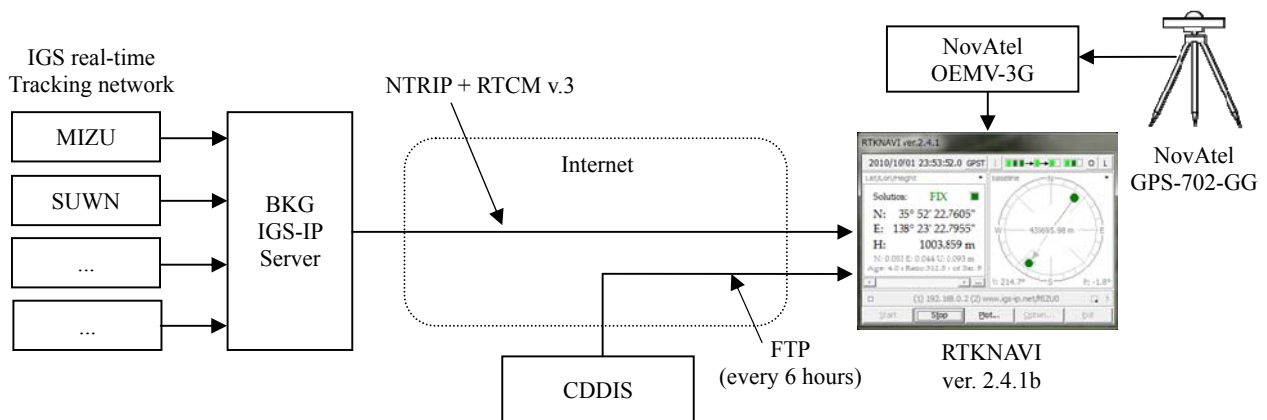


Figure 6. Configuration of the real-time test for the long baseline RTK strategy.

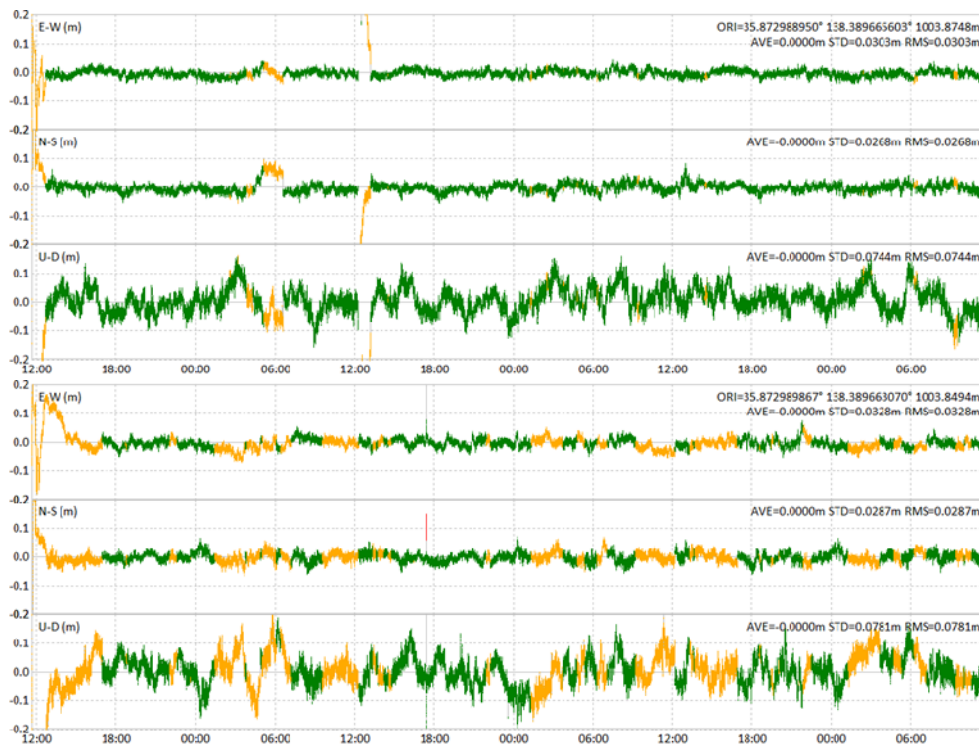


Figure 8. Real-time test results for long baseline RTK strategy as E/N/U error plots of 1 Hz solutions for 72 hours (upper: base station=MIZU, baseline length=435.7 km, lower: base station= SUWN, baseline length=1024.8 km)

According to the test results, both of the precision of the RTK solutions and the fixing ratio in real-time environment were worth than the offline results in summer time. A reason of the degradation of the long baseline RTK solutions is considered the latency of the base station data. In this real-time, the latency of the real-time streams of the base station data was 1 s to 6 s. It often took over 10 s. The latency the data transmission between the rover and the base station derives the additional errors caused by the satellite onboard clock drift and ionosphere temporal variation of ionosphere or troposphere. Another possibility is miss-modeling of measurement errors. In the current long baseline RTK strategy, the errors at different epochs are not assumed to have any correlation each other. In the condition with the sampling interval 30 s for the offline test, the correlation can be generally neglected. With the sampling interval of 1 s, however, the correlation is not negligible. More realistic modeling for such time-correlated measurement errors is necessary for such higher sampling rate. In addition to the latency and the time-correlation, the multipath effect of the rover antenna is also one of the possibilities of the performance degradation. Further investigation the details of error sources are needed to improve the long baseline RTK in real-time environment.

CONCLUSION AND FUTURE WORKS

In this study, we proposed a new strategy for the long baseline RTK up to 1,000 km baseline without generating any linear combination of measurement of GNSS signals. The strategy also includes an integer ambiguity resolution optimized for long baseline RTK with existing error sources. To verify and demonstrate the strategy, we conducted some tests in various baseline lengths up to 1,100 km both in offline mode and real-time mode. According to the test results, the proposed strategy for long baseline RTK works well. The solutions, however, are degraded in summer time. And real-time case is harder to get better solutions than offline test. Further investigation and improvement are necessary to establish the more reliable and practical strategy for long baseline RTK.

ACKNOWLEDGEMENTS

The authors are very grateful to IGS for providing high quality precise ephemerides as well as real-time observation data of tracking stations world-wide.

REFERENCES

- [1] B.Hofmann-Wellenhof, H.Lichtenegger and J.Collins, Global Positioning System: Theory and Practice, Fifth revised edition, Springer Wien NewYork, 2001
- [2] H.J.Euler, C.R.Keenan, B.E.Zebhause, Study of a simplified approach in utilizing information from permanent reference station arrays, ION GPS 2001
- [3] T.Kato, Y.Terada, M.Kinosita, H.Kakimoto, H.Issiki, T.Moriguchi, M.Takada, T.Tanno, M. Kanzaki and J.Johnson, A new tsunami monitoring system using RTK-GPS, proceeding of ITS 2001
- [4] P.J.G.Teunissen, The least-square ambiguity decorrelation adjustment: a method for fast GPS ambiguity estimation, J.Geodesy, vol.70, 1995
- [5] G.Blewitt, Carrier phase ambiguity resolution for the global positioning system applied to geodetic baselines up to 2000 km, Journal of Geophysical Research, Vol. 94, 1989
- [6] Gelb ed., Applied Optimal Estimation, The M.I.T. Press, London, 1974
- [7] X.-W.Chang, X.Yang and T.Zhou, MLAMBDA: A modified LAMBDA method for integer least-squares estimation, J.Geodesy, vol.79, 2005
- [8] T.Takasu, and A.Yasuda, Development of the low-cost RTK-GPS receiver with an open source program package RTKLIB, International Symposium on GPS/GNSS 2009, ICC Jeju, Korea
- [9] RTCM recommended standards for differential GNSS (global navigation satellite systems) service version 2.3, August 20, 2001, RTCM SC-104
- [10] RTCM standard 10403.1 for differential GNSS (global navigation satellite systems) service - version 3, October 27, 2006, RTCM SC-104
- [11] RTCM recommended standards for networked transport of RTCM via internet protocol (NTRIP) version 1.0, September 30, 2004, RTCM SC-104
- [12] J.M.Dow, R.E.Neilan, and C.Rizos, The International GNSS Service in a changing landscape of Global Navigation Satellite Systems, Journal of Geodesy, 2009
- [13] W.Gurtner and L.Estey, RINEX the receiver independent exchange format version 3.00, November 28, 2007
- [14] RTKLIB: An open source program package for GNSS positioning, <http://www.rtklib.com>
- [15] T.Sagiya, A decade of GEONET: 1994-2003 - The continuous GPS observation in Japan and its impact on earthquake studies, Earth Planets Space, Vol. 56, 2004